



## Direct Visualization of Independent Ta Centers Supported on Two-Dimensional TiO<sub>2</sub> Nanosheets

Bo, Z., Thornburg, N. E., Peng, L., Moreno, J. J. G., Nolan, M., Marks, L. D., & Notestein, J. M. (2019). Direct Visualization of Independent Ta Centers Supported on Two-Dimensional TiO<sub>2</sub> Nanosheets. *Nano Letters*, 19(11), 8103-8108. <https://doi.org/10.1021/acs.nanolett.9b03305>

[Link to publication record in Ulster University Research Portal](#)

**Published in:**  
Nano Letters

**Publication Status:**  
Published (in print/issue): 29/10/2019

**DOI:**  
[10.1021/acs.nanolett.9b03305](https://doi.org/10.1021/acs.nanolett.9b03305)

**Document Version**  
Author Accepted version

### General rights

Copyright for the publications made accessible via Ulster University's Research Portal is retained by the author(s) and / or other copyright owners and it is a condition of accessing these publications that users recognise and abide by the legal requirements associated with these rights.

### Take down policy

The Research Portal is Ulster University's institutional repository that provides access to Ulster's research outputs. Every effort has been made to ensure that content in the Research Portal does not infringe any person's rights, or applicable UK laws. If you discover content in the Research Portal that you believe breaches copyright or violates any law, please contact [pure-support@ulster.ac.uk](mailto:pure-support@ulster.ac.uk).

# Direct Visualization of Independent Ta Centers supported on 2D TiO<sub>2</sub> nanosheets

Zhenyu Bo<sup>1</sup>, Nick Thornburg<sup>2</sup>, Lingxuan Peng<sup>1</sup>, Jose Julio Gutierrez Moreno<sup>3</sup>, Michael Nolan<sup>3</sup>, Laurence D. Marks<sup>1</sup>, Justin M. Notestein<sup>2\*</sup>

1. Department of Materials Science and Engineering, Northwestern University, Evanston, IL, 60208
2. Department of Chemical and Biological Engineering, Northwestern University, Evanston, IL, 60208
3. Tyndall National Institute, University College Cork, Lee Maltings, Dyke Parade, Cork, Ireland

\* Corresponding author email: j-notestein@northwestern.edu

## ABSTRACT

Highly-dispersed, supported oxides are ubiquitous solid catalysts, but they can be challenging to characterize with atomic precision. Here it is shown that crystalline anatase TiO<sub>2</sub> nanosheets (~5 nm thick) are ideal supports for imaging highly-dispersed active sites. Ta cations are deposited by several routes, and high-resolution high angle annular dark-field (HAADF) scanning transmission electron microscopy (STEM) is used to determine the location of Ta with respect to the TiO<sub>2</sub> lattice and to quantify Ta-Ta distances. In the best case, it is shown that >80% of Ta atoms are isolated from one another, whereas other techniques are blind to this critical catalytic property or give only qualitative estimates. TiO<sub>2</sub> nanosheets may prove to be a useful platform for other types of catalysis studies.

## KEYWORDS

HAADF STEM; supported catalysts; oxides; microscopy; single atom catalysts

Heterogeneous catalysts are solid materials that catalyze reactions in the gas or liquid phase, and are essential in chemicals manufacturing, fuels production and emissions control.<sup>1,2</sup> They take a variety of forms including supported metal nanoparticles such as Pt/Al<sub>2</sub>O<sub>3</sub> for hydrogenation/dehydrogenation or combustion,<sup>3</sup> bulk oxides such as the complex MoVTaNbO materials used in ammoxidation,<sup>4</sup> or supported metal oxides such as TiO<sub>x</sub>/SiO<sub>2</sub> and VO<sub>x</sub>/TiO<sub>2</sub>.<sup>5,6</sup> This last category is frequently used in reactions such as the selective oxidation of alcohols and alkenes, emissions control, and photocatalysis.<sup>7-10</sup>

The reactivity of any heterogeneous catalyst is dependent on the number of the active atoms (e.g. Ti atoms in TiO<sub>x</sub>/SiO<sub>2</sub> catalysts) that are accessible to the reactants.<sup>6, 11, 12</sup> To keep this value as high as possible, catalysts are typically synthesized to be as dispersed as possible while retaining their active form, giving oxide domains that are ideally present as single cations on the support, small clusters, or monolayers. In addition, supported oxides are also well-known to be 'structure-sensitive', in that their precise atomic connectivity to other active atoms and to the support has a large impact on catalytic rates and selectivities.<sup>13-16</sup>

Therefore, the catalysis community is continuously looking for methods to control the chemical environment and the dispersion of active sites during the synthesis of supported metal oxide catalysts. These methods can include the use of bulky or well-defined precursors to enforce site-isolation,<sup>17, 18</sup> multinuclear precursors to create small clusters,<sup>19-21</sup> thermolytic molecular precursors,<sup>22, 23</sup> substituted silsesquioxanes,<sup>23, 24</sup> atomic layer deposition,<sup>25-27</sup> and engineered supports,<sup>28-30</sup> among many other approaches.

Beyond the synthesis, a significant challenge in supported oxides of all types is characterizing them with atomic precision. Historically, characterization of the active sites of supported oxide catalysts has been via probe reactions and via X-ray absorption, UV-visible, NMR, vibrational, and other spectroscopies. However, these techniques all give local properties of the probed atom, and are also averaged over the whole sample, making it

challenging to tease out some of the finer details of synthesis-structure-function relationships, such as the distribution of atoms across a surface. Finally, chemical site counting methods can provide distributions of the properties of active sites,<sup>31, 32</sup> but do not necessarily provide structural information.

Significant advances have been made in recent years for the direct, atomic-level visualization of supported catalyst active sites by electron microscopy, even as the active sites themselves trend towards single-atom dimensions.<sup>33, 34</sup> However, there remain several significant limitations. First, most imaging of single-atom and small cluster catalysts has occurred with 3<sup>rd</sup> row, low-valent, late transition metals (eg. Au, Pt, Ir).<sup>33-35</sup> These elements provide good Z-contrast and are widely used catalysts. In contrast, supported, high-valent, early transition metal cations and oxides have not been the target of these types of imaging studies, likely because the 1<sup>st</sup> row elements are more commonly used in catalysis within these groups. Second, zeolites and other crystalline oxides like SrTiO<sub>3</sub> have been preferred for atomic-resolution imaging of supported species, in part because of the relative ease of imaging along a particle edge on such supports.<sup>36, 37</sup> It is more challenging to image species with atomic resolution on the surface of traditional, high surface areas supports such as Al<sub>2</sub>O<sub>3</sub>, TiO<sub>2</sub> and SiO<sub>2</sub> because of their amorphous or highly faceted surfaces and relatively large primary particles. There have been successes using core-shell or very small support oxide particles to image and locate single catalyst atoms,<sup>38, 39</sup> but it remains very challenging to focus highly converged electron beams on more than a small area at a time.

In this letter, we report the use of 2D TiO<sub>2</sub> nanosheets (nsTiO<sub>2</sub>) as nearly ideal support materials for the direct visualization of highly-dispersed catalysts across large particle surface areas. Here, we demonstrate its utility for tantalum oxides (TaO<sub>x</sub>/TiO<sub>2</sub>) to address the dearth of imaging of supported, high-valent, early transition metal cations, but these supports should be generally applicable for imaging supported catalysts. The use of thin (~5 nm), flat, anatase

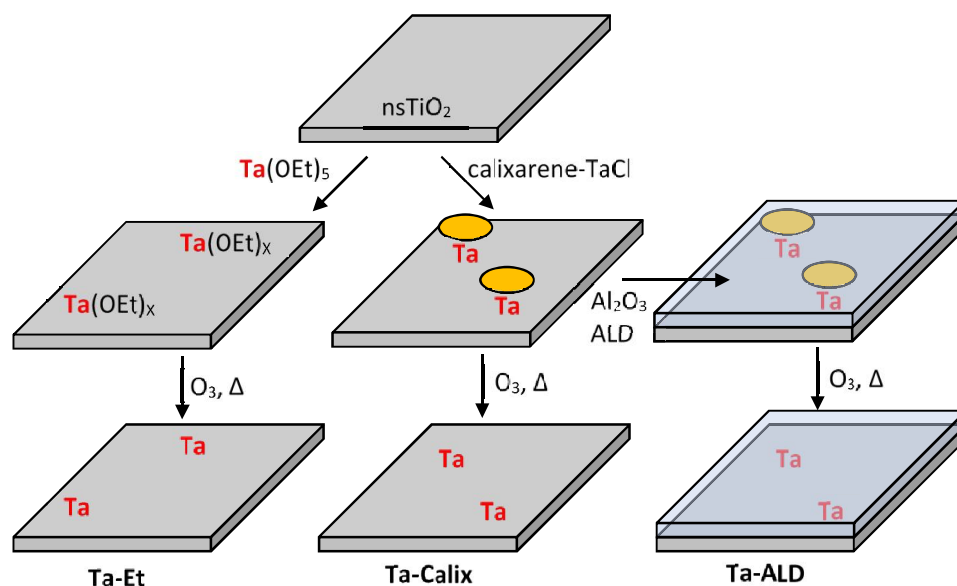
1  
2  
3 TiO<sub>2</sub> nanosheets instead of traditional oxide particles makes it possible to keep the entire  
4 surface in focus during High-Resolution High Angle Annular Dark-Field (HAADF) imaging,  
5 rather than very small regions on a particle edge, as is typical for conventional supports.  
6  
7 Moreover, in contrast to prior examples of STEM,<sup>40</sup> STM,<sup>41, 42</sup> or atom-probe tomography,<sup>43</sup>  
8 high surface area powders are used here, permitting bulk characterization tools to be used on  
9 the same material with no special modifications. Second- and third-row highly dispersed metal  
10 oxides are less commonly used than their first-row counterparts, but have recently gained  
11 attention for having comparable, or in many cases greater, activity or selectivity in a variety of  
12 thermochemical transformations.<sup>7, 15</sup> TaOx-based materials have been shown to be interesting  
13 in a variety of selective oxidation reactions,<sup>44-46</sup> and Ta-TiO<sub>2</sub> specifically is of interest as an  
14 acid catalyst<sup>47</sup> and for its photocatalytic properties.<sup>48-50</sup>

15  
16 The images collected here provide direct evidence for single-atom dispersion and  
17 provide the distribution of Ta-Ta nearest-neighbor distances over a wide area, giving insight  
18 into the sensitivity of the TaOx structure on the Ta precursor used for synthesis. It also gives  
19 insight into the effects of post-synthetic modifications, such as subsequent atomic layer  
20 deposition of an additional oxide. Precursor and post-synthesis modification have both been  
21 shown to strongly influence the catalyst activity and stability,<sup>25, 30, 51</sup> but as mentioned above,  
22 direct connections to surface speciation have remained elusive.

23  
24 TiO<sub>2</sub> nanosheets (nsTiO<sub>2</sub>) were synthesized using titanium butoxide and hydrofluoric  
25 acid under autoclave conditions following previously reported procedures.<sup>52</sup> The N<sub>2</sub>  
26 physisorption specific surface area measured (Supporting Information Figure S1) by the BET  
27 method is 145 m<sup>2</sup>/g. These materials consist of platelets with particle dimensions of length and  
28 width below 100 nm and thickness below 10 nm (SI Figure S2) Typical particles have length  
29 and width of ~60 nm and a thickness of ~ 5 nm. These materials have pure anatase phase, with  
30 X-ray diffraction peaks corresponding to the (101), (004), (200), (105) and (211) crystal planes

(SI Figure S3).<sup>53</sup> The particles are not annealed, and the large faces are unreconstructed and [001]-terminated.<sup>52</sup> The particles are flat for imaging over extended distances, but the faces are not atomically smooth and are expected to contain the types of surface defects found in other TiO<sub>2</sub> materials.

To deposit Ta atoms, (illustrated in Scheme 1), nsTiO<sub>2</sub> was dispersed in a toluene solution containing either calixarene-TaCl (30mM, 40mL, ultimately giving material **Ta-Calix**)<sup>54</sup> as a representative bulky precursor previously shown to help enforce site-isolation on silica, or Ta(OEt)<sub>5</sub> (Sigma-Aldrich, 15mM, 10mL, ultimately giving materials **Ta-Et**) and the solution was heated to reflux for 24 h. The modified nsTiO<sub>2</sub> was washed with anhydrous toluene and dried under dynamic vacuum at room temperature. This procedure grafts the Ta atoms at a surface density of ~0.3 Ta nm<sup>-2</sup>, or 70 μmol Ta g<sup>-1</sup> as determined by thermogravimetric analysis (to measure calixarene ligand content, SI Figure S4) and ICP-OES (Ta content). This loading was chosen because it is approximately the geometrical limit resulting from the large calixarene ligand.<sup>25</sup> Some samples of as-synthesized **Ta-Calix** were coated with <1 nm Al<sub>2</sub>O<sub>3</sub> using atomic layer deposition (ALD) of five alternating cycles of Al(CH<sub>3</sub>)<sub>3</sub> and H<sub>2</sub>O,<sup>25</sup> ultimately leading to material **Ta-ALD**. Finally, all samples were treated in flowing O<sub>3</sub> at 110°C to remove any residual organic ligands. In addition to electron microscopy, samples were also characterized by X-ray diffraction (XRD) and X-ray photoelectron (XPS), diffuse reflectance UV-visible (DRUV-vis), and Raman spectroscopies. See SI for full procedures.



**Scheme 1.** Modification of anatase 001-terminated  $\text{TiO}_2$  nanosheets ( $\text{nsTiO}_2$ ) with Ta and with an  $\text{Al}_2\text{O}_3$  overcoat

HAADF imaging was completed using a JEOL JEM-ARM200CF aberration-corrected scanning transmission electron microscope. To prepare the sample for imaging, ethanol suspensions of samples were drop-cast onto TEM grids and air-dried. The HAADF images were acquired using a probe of  $\sim 0.078$  nm, an emission current of  $15 \mu\text{A}$  and a beam current of  $\sim 19\text{pA}$  with a  $40 \mu\text{m}$  condenser lens aperture. The collection angle of the HAADF was greater than  $80$  degrees. Ta atom nearest neighbor distances (NND) were calculated using Image J software.

Conventional spectroscopies and other characterization tools are often limited in the information they can provide for mixed or supported oxides, as they give ensemble averages of the materials. XRD after Ta deposition or after ALD (SI Figure S3) shows no changes or additional features. This indicates that neither did a  $\text{TaO}_x$  crystal phase form on top of the  $\text{nsTiO}_2$  nor did Ta insert into the  $\text{TiO}_2$  lattice to any significant extent, but it provides no information on the actual  $\text{TaO}_x$  structure adopted. XPS (SI Figure S5) shows binding energy peaks at  $458.6$  eV and  $464.5$  eV in the Ti 2p region and at  $530.5$  eV in the O 1s region, which are typical of  $\text{Ti}^{4+}$  and oxygen ions in metal oxides.<sup>53</sup> The Ta 4f peaks around  $26$  eV and  $28$  eV

confirm the presence of Ta with high oxidation state in the Ta-containing samples.<sup>55, 56, 57</sup> The absence of observable features near 855 cm<sup>-1</sup> in the Raman spectrum could indicate the absence of Ta-O-Ta bonds that would be found in larger clusters.<sup>58</sup> However, as is often the case with supported oxide catalysts, stronger conclusions are precluded by the relatively low loadings of Ta and the strong contribution from nsTiO<sub>2</sub> itself. Likewise, DRUV-vis can be a useful tool for characterizing supported oxides,<sup>6, 7</sup> but here cannot distinguish the Ta-containing materials from the parent nsTiO<sub>2</sub> (SI Figure S7). Overall, XRD, XPS and Raman studies confirm the presence of small amounts of highly dispersed Ta oxide on anatase nsTiO<sub>2</sub> but cannot provide further details.

Therefore, high-resolution HAADF-STEM images were acquired to enable direct observation of the distribution of Ta atoms on the TiO<sub>2</sub> surface with atomic resolution. Figure 1a) shows the structure of **Ta-Et** taken along the [001] direction of the nsTiO<sub>2</sub> crystallite. The image clearly demonstrates that the Ta atoms are located on top of the Ti-O columns, and there were no Ta atoms located between columns. This alignment requires that the Ta atoms were present either directly above the Ti lattice sites, or as substitutions for Ti atoms within the lattice or at the surface. Because of the synthesis method and the mild post-synthesis treatments, it is most likely that Ta grafts directly above the Ti atoms. Density functional theory (see SI for details) confirms that, regardless of the extents of Ta atom hydration and surface hydroxylation, the stable configuration places Ta atoms directly above a Ti atom column, as illustrated in Figure 1b) and Figure 1c). We note that the Ta atoms occupy different crystallographic positions depending on the state of hydration, although we cannot verify this from the microscopy. The circles in Figure 1a) highlight some of the many isolated Ta atoms (no Ta atoms at the neighboring lattice position) in this sample. The squares in Figure 1 show some potential pairs or oligomers of Ta atoms at adjacent sites.



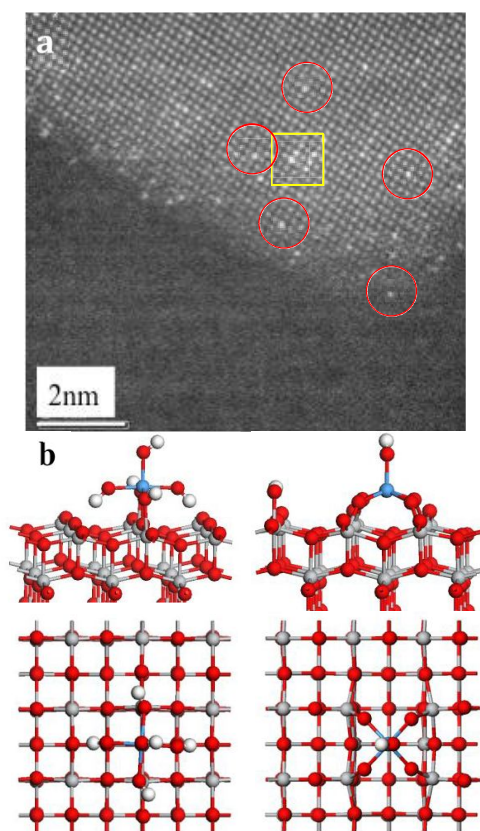


**Figure 1.** a) High-resolution HAADF-STEM image of sample **Ta-Et** acquired along the [001] direction of the TiO<sub>2</sub> support. A median filter with a window of size 2 was applied to this image. The unprocessed image is given in SI Figure S8. The bright dots are individual Ta atoms. Red circles highlight isolated Ta atoms and the yellow square highlights potential regions where Ta atoms are found in adjacent sites, b) optimized structures of Ta<sup>5+</sup> supported on a TiO<sub>2</sub> anatase (001) surface generated using density functional theory modeling showing alignment of Ta with Ti columns, whether fully hydrated (left) or dehydrated (right); see SI for discussion. Red = O, gray = Ti, blue = Ta, white = H.

Next, the unique ability to locate Ta atoms over longer distances on nsTiO<sub>2</sub> is used to map out Ta-Ta distances for the materials. Figure 2 shows a representative set of atomic resolution HAADF-STEM images of **Ta-Et**, **Ta-Calix** and **Ta-ALD** taken in plan-view to obtain information about Ta-Ta spacing. Because of the planar supports, single images provide information representative of the entire sample. For example, Figure 2d shows 186 atoms over approximately 350 nm<sup>2</sup> of imaged area (700 nm<sup>2</sup> of TiO<sub>2</sub> surface). This gives 3.7 nm<sup>2</sup> Ta<sup>-1</sup>, in good agreement with the specific surface area of the nsTiO<sub>2</sub> divided by the total amount of Ta

grafted ( $3.3 \text{ nm}^2 \text{ Ta}^{-1}$ ). From visual inspection alone, the two Ta precursors do not produce markedly different Ta distributions on the surface, with many isolated atoms in both cases. In addition, the Ta distribution is not apparently changed by  $\text{Al}_2\text{O}_3$  overcoating by ALD. The ALD process utilizes the very reactive molecule  $\text{Al}(\text{CH}_3)_3$  and generates water vapor at moderate temperatures, and it was initially suspected that the process might significantly rearrange the surface TaOx. We also note that while the nsTiO<sub>2</sub> supports can be damaged by long electron beam exposures, the Ta remain as single atoms, with no obvious changes to their orientation with respect to the TiO<sub>2</sub> surface. (Figure S9a and b) This contrasts with control materials such as Ta on silica nanospheres, in which the Ta is challenging to visualize initially then obviously aggregates during microscopy. (Figure S9c and d)

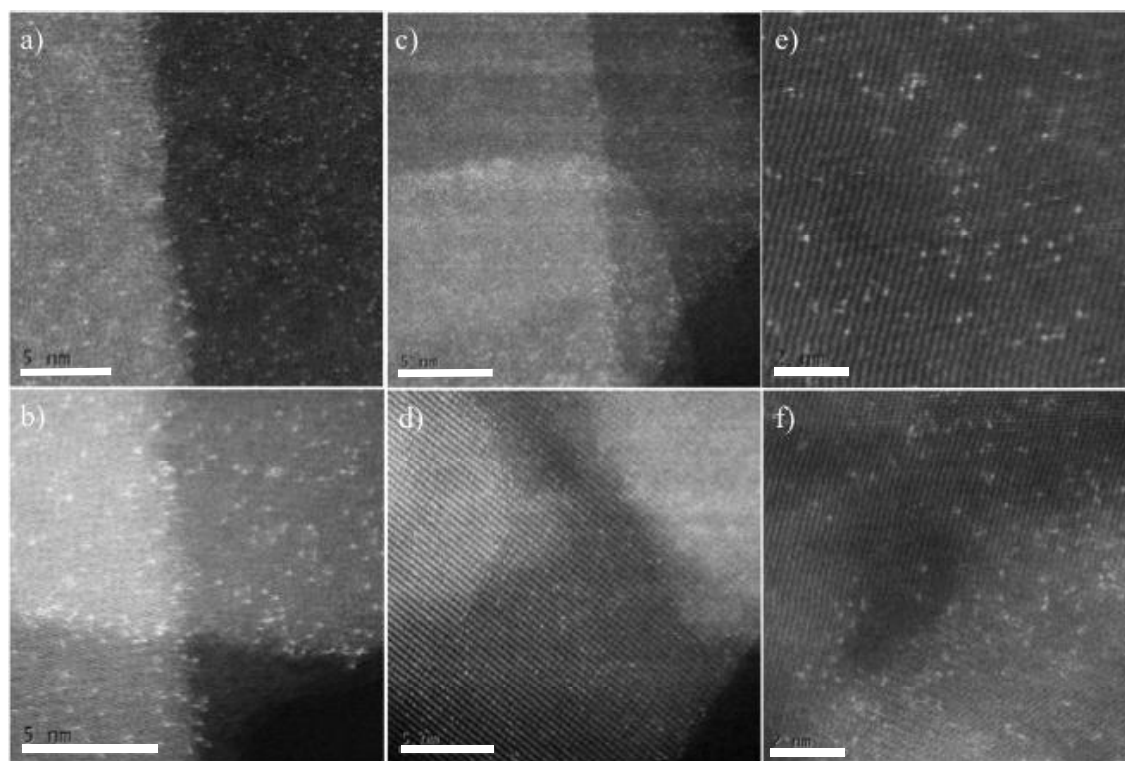


**Figure 2.** Representative high resolution HAADF-STEM images of a,b) **Ta-Calix**, c,d) **Ta-Et**, e,f) **Ta-ALD**. Scale bars in a-d are 5 nm. Scale bars in e and f are 2 nm.

These images enabled by the extended, flat surface of nsTiO<sub>2</sub> allows for statistically meaningful estimates ( $N = 134\text{--}186$  Ta atoms) of the distribution of supported Ta atoms from a small number of images. The observed nearest neighbor distances (NND) are calculated for all visible Ta atoms in Figure 2 (see also SI Figure S10). The median NND for materials **Ta-Et**, **Ta-Calix**, and **Ta-ALD** are 0.5, 0.7, and 0.5 nm. From the  $3.3\text{ nm}^2\text{ Ta}^{-1}$  average loading, Ta perfectly dispersed on the surface would have an apparent Ta-Ta separation of 0.9 nm. We also quantitatively estimate the fraction of Ta atoms that are 'isolated' from another, by placing a cutoff Ta-Ta separation of  $>0.4$  nm from the nearest neighbor, approximately the Ta-O-Ta distance in Ta<sub>2</sub>O<sub>5</sub>.<sup>59</sup> The cumulative frequency distributions in Figure 3 show that for all materials,  $>60\%$  of Ta atoms are isolated from each other, with potentially  $>80\%$  of the Ta atoms being isolated in the case of **Ta-Calix**, which is derived from the bulky precursor. It is emphasized that these estimates are conservative. Because the imaging technique visualizes all Ta atoms in a 2D space, Ta atoms sitting on the other side of the TiO<sub>2</sub> nanosheets were also imaged, thus increasing the apparent Ta surface density.

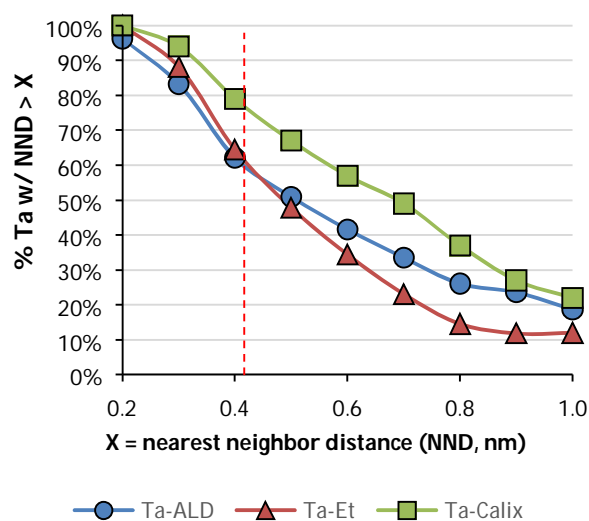


**Figure 3.** Cumulative frequency plot of nearest neighbor distance (NND, Ta to Ta distance in nm) for samples **Ta-Et** (186 atoms counted), **Ta-Calix** (134 atoms counted) and **Ta-ALD** (161 atoms counted). Ta to Ta distances  $\leq 0.4$  nm, indicated by the red line, might indicate the formation of Ta-O-Ta bonds.

‘Isolated’ sites have long been argued from spectroscopy to be the most active sites in a number of reactions,<sup>35,60</sup> and many synthetic methods, including the use of bulky ligands such as calixarene,<sup>54,25</sup> have been specifically developed to bias the system towards a preponderance of these sites. For the first time, we have directly demonstrated the validity of these claims from HAADF-STEM imaging. Recalling that **Ta-ALD** is derived from the same precursor material as **Ta-Calix**, the full analysis of the Ta-Ta distances also shows that the conditions of the ALD indeed cause some rearrangement and aggregation of TaOx, even if the aggregation is not severe enough to be observed by bulk techniques. In conclusion, we have demonstrated the use of TiO<sub>2</sub> nanosheets as excellent 2D supports for high resolution STEM imaging of highly-dispersed, supported catalysts and quantification of atom-atom distance distributions. We are currently working to apply this technique to other catalytic metals and systems.

## ASSOCIATED CONTENT

**Supporting Information.** Materials synthesis procedures; characterization: N<sub>2</sub> physisorption, XRD, TGA, XPS, Raman, UV-visible; additional TEM and Ta-Ta distance histograms; computational details and results

## Corresponding Author

\*Email for J.M.N.: j-notestein@northwestern.edu

## Notes

The authors declare no competing financial interest.

## Acknowledgements

This material is based upon work supported by the U.S. Department of Energy, Office of Science, Office of Basic Energy Science, under Award Number DOE DE-FG02-03ER15457 to the Institute for Catalysis for Energy Processes (ICEP) at Northwestern University. This

work was supported by the Materials Research Center (MRSEC) at Northwestern University, on grant number DMR-112126. N.E.T. and J.M.N. acknowledge financial support from the Dow Chemical Company. This work made use of the EPIC facility of the NUANCE Center at Northwestern University, which has received support from the Soft and Hybrid Nanotechnology Experimental (SHyNE) Resource (NSF NNCI-1542205); the MRSEC program (NSF DMR-112126) at the Materials Research Center; the International Institute for Nanotechnology (IIN); the Keck Foundation; and the State of Illinois, through the IIN. This work made use of the JEOL JEM-ARM200CF in the Electron Microscopy Service [Research Resources Center, University of Illinois at Chicago (UIC)]. JJGM and MN acknowledge support from the Irish Environmental Protection Agency UisceSense project (W-2015-MS-21) and the SFI-NSF-DEL US Ireland R&D Partnership Program, grant number SFI US/14/e2915 and access to computational resources through the Irish Center for High End Computing. We acknowledge supply of raw materials (TiO<sub>2</sub> nanosheets) by Dr. Kevin Schwartzberg (Northwestern University) and atomic layer deposition work by Cassie George (Northwestern University).

## References

1. Satterfield, C. N., *Heterogeneous Catalysis in Industrial Practice*. 2nd Edition. 1991.
2. Mizuno, N.; Misono, M. *Chem. Rev.* **1998**, 98, 199-218.
3. Stanislaus, A.; Cooper, B. H. *Catalysis Reviews—Science and Engineering* **1994**, 36, 75-123.
4. Millet, J.; Roussel, H.; Pigamo, A.; Dubois, J.; Jumas, J. *Appl. Catal. A: Gen.* **2002**, 232, 77-92.
5. Olthof, B.; Khodakov, A.; Bell, A. T.; Iglesia, E. *J. Phys. Chem. B* **2000**, 104, 1516-1528.
6. Gao, X.; Wachs, I. E. *Catal. Today* **1999**, 51, 233-254.
7. Thornburg, N. E.; Thompson, A. B.; Notestein, J. M. *ACS Catal.* **2015**, 5, 5077-5088.
8. Wachs, I. E. *Dalton Trans.* **2013**, 42, 11762-11769.
9. Mallat, T.; Baiker, A. *Chem. Rev.* **2004**, 104, 3037-3058.
10. Clerici, M.; Bellussi, G.; Romano, U. *J. Catal.* **1991**, 129, 159-167.
11. Xu, Z.; Xiao, F.-S.; Purnell, S.; Alexeev, O.; Kawi, S.; Deutsch, S.; Gates, B. *Nature* **1994**, 372, 346-348.
12. Van Santen, R. A. *Acc. Chem. Res.* **2008**, 42, 57-66.
13. Weckhuysen, B. M.; Keller, D. E. *Catal. Today* **2003**, 78, 25-46.

14. Grant, J. T.; Carrero, C. A.; Love, A. M.; Verel, R.; Hermans, I. *ACS Catal.* **2015**, 5, 5787-5793.
15. Onfroy, T.; Clet, G.; Houalla, M. *J. Phys. Chem. B* **2005**, 109, 14588-14594.
16. Tian, H.; Ross, E. I.; Wachs, I. E. *J. Phys. Chem. B* **2006**, 110, 9593-9600.
17. Prieto-Centurion, D.; Notestein, J. M. *J. Catal.* **2011**, 279, 103-110.
18. Jarupatrakorn, J.; Tilley, T. D. *J. Am. Chem. Soc.* **2002**, 124, 8380-8388.
19. Wegener, S. L.; Marks, T. J.; Stair, P. C. *Acc. Chem. Res.* **2011**, 45, 206-214.
20. Wegener, S. L.; Kim, H.; Marks, T. J.; Stair, P. C. *J. Phys. Chem. Lett.* **2011**, 2, 170-175.
21. Hess, C.; Hoefelmeyer, J. D.; Tilley, T. D. *J. Phys. Chem. B* **2004**, 108, 9703-9709.
22. Fujdala, K. L.; Tilley, T. D. *J. Catal.* **2003**, 216, 265-275.
23. Nozaki, C.; Lugmair, C. G.; Bell, A. T.; Tilley, T. D. *J. Am. Chem. Soc.* **2002**, 124, 13194-13203.
24. Duchateau, R. *Chem. Rev.* **2002**, 102, 3525-3542.
25. Canlas, C. P.; Lu, J.; Ray, N. A.; Grosso-Giordano, N. A.; Lee, S.; Elam, J. W.; Winans, R. E.; Van Duyne, R. P.; Stair, P. C.; Notestein, J. M. *Nature Chem.* **2012**, 4, 1030-6.
26. Liu, R.; Lin, Y.; Chou, L. Y.; Sheehan, S. W.; He, W.; Zhang, F.; Hou, H. J.; Wang, D. *Angew. Chem.* **2011**, 123, 519-522.
27. Herrera, J. E.; Kwak, J. H.; Hu, J. Z.; Wang, Y.; Peden, C. H. *Top. Catal.* **2006**, 39, 245-255.
28. Thomas, J. M.; Hernandez-Garrido, J. C.; Raja, R.; Bell, R. G. *Phys. Chem. Chem. Phys.* **2009**, 11, 2799-2825.
29. Chal, R.; Gérardin, C.; Bulut, M.; Van Donk, S. *ChemCatChem* **2011**, 3, 67-81.
30. Gao, X.; Wachs, I. E. *Top. Catal.* **2002**, 18, 243-250.
31. Eaton, T. R.; Boston, A. M.; Thompson, A. B.; Gray, K. A.; Notestein, J. M. *ChemCatChem* **2014**, 6, 3215-3222.
32. Eaton, T. R.; Campos, M. P.; Gray, K. A.; Notestein, J. M. *J. Catal.* **2014**, 309, 156-165.
33. Ding, K.; Gulec, A.; Johnson, A. M.; Schweitzer, N. M.; Stucky, G. D.; Marks, L. D.; Stair, P. C. *Science* **2015**, 350, 189-192.
34. Fu, Q.; Saltsburg, H.; Flytzani-Stephanopoulos, M. *Science* **2003**, 301, 935-938.
35. Kistler, J. D.; Chotigkrai, N.; Xu, P.; Enderle, B.; Praserthdam, P.; Chen, C. Y.; Browning, N. D.; Gates, B. C. *Angew. Chem.* **2014**, 126, 9050-9053.
36. Flytzani-Stephanopoulos, M.; Gates, B. C. *Ann. Rev. Chem. Biomol. Eng.* **2012**, 3, 545-574.
37. Chen, B.-R.; Crosby, L. A.; George, C.; Kennedy, R. M.; Schweitzer, N. M.; Wen, J.; Van Duyne, R. P.; Stair, P. C.; Poeppelmeier, K. R.; Marks, L. D.; Bedzyk, M. J. *ACS Catal.* **2018**, 8, 4751-4760.
38. DeRita, L.; Resasco, J.; Dai, S.; Boubnov, A.; Thang, H. V.; Hoffman, A. S.; Ro, I.; Graham, G. W.; Bare, S. R.; Pacchioni, G.; Pan, X.; Christopher, P. *Nature Mater.* **2019**, 18, 746-751.
39. Lee, B.-H.; Park, S.; Kim, M.; Sinha, A. K.; Lee, S. C.; Jung, E.; Chang, W. J.; Lee, K.-S.; Kim, J. H.; Cho, S.-P.; Kim, H.; Nam, K. T.; Hyeon, T. *Nature Mater.* **2019**, 18, 620-626.
40. Chang, T.-Y.; Tanaka, Y.; Ishikawa, R.; Toyoura, K.; Matsunaga, K.; Ikuhara, Y.; Shibata, N. *Nano Lett.* **2014**, 14, 134-138.
41. Fernandez-Garcia, M.; Martinez-Arias, A.; Hanson, J.; Rodriguez, J. *Chem. Rev.* **2004**, 104, 4063-4104.
42. Bell, A. T. *Science* **2003**, 299, 1688-1691.
43. Buurmans, I. L.; Weckhuysen, B. M. *Nature Chem.* **2012**, 4, 873-886.
44. Morlanes, N.; Notestein, J. M. *J. Catal.* **2010**, 275, 191-201.
45. Nauert, S. L.; Savereide, L.; Notestein, J. M. *ACS Catal.* **2018**, 8, 7598-7607.

46. Avenier, P.; Taoufik, M.; Lesage, A.; Solans-Monfort, X.; Baudouin, A.; de Mallmann, A.; Veyre, L.; Basset, J. M.; Eisenstein, O.; Emsley, L.; Quadrelli, E. A. *Science* **2007**, 317, 1056-1060.
47. Chen, Y. S.; Fierro, J. L. G.; Tanaka, T.; Wachs, I. E. *J. Phys. Chem. B* **2003**, 107, 5243-5250.
48. Visinescu, C. M.; Sanjines, R.; Lévy, F.; Marcu, V.; Pârvulescu, V. I. *J. Photochem. Photobiol. A: Chem.* **2005**, 174, (2), 106-112.
49. Baiju, K. V.; Shajesh, P.; Wunderlich, W.; Mukundan, P.; Kumar, S. R.; Warriar, K. G. *J. Mol. Catal. A* **2007**, 276, (1), 41-46.
50. Feng, X.; Shankar, K.; Paulose, M.; Grimes, C. A. *Angew. Chem. Int. Ed.* **2009**, 48, (43), 8095-8098.
51. Iglesia, E. *Appl. Catal. A: Gen.* **1997**, 161, (1-2), 59-78.
52. Liang, Y. T.; Vijayan, B. K.; Lyandres, O.; Gray, K. A.; Hersam, M. C. *J. Phys. Chem. Lett.* **2012**, 3, (13), 1760-1765.
53. Södergren, S.; Siegbahn, H.; Rensmo, H.; Lindström, H.; Hagfeldt, A.; Lindquist, S.-E. *J. Phys. Chem. B* **1997**, 101, (16), 3087-3090.
54. Morlanés, N.; Notestein, J. M. *J. Catal.* **2010**, 275, (2), 191-201.
55. Masuda, Y.; Wakamatsu, S.; Koumoto, K. *J. Eur. Ceram. Soc.* **2004**, 24, (2), 301-307.
56. Liu, J.; Yang, H.; Tan, W.; Zhou, X.; Lin, Y. *Electrochim. Acta* **2010**, 56, (1), 396-400.
57. Liu, X.; Wu, X.; Scott, K. *Catal. Sci. Technol.* **2014**, 4, (11), 3891-3898.
58. Chen, Y.; Fierro, J. L.; Tanaka, T.; Wachs, I. E. *J. Phys. Chem. B* **2003**, 107, (22), 5243-5250.
59. Takahara, Y.; Kondo, J. N.; Takata, T.; Lu, D.; Domen, K. *Chem. Mater.* **2001**, 13, (4), 1194-1199.
60. Yang, M.; Allard, L. F.; Flytzani-Stephanopoulos, M. *J. Am. Chem. Soc.* **2013**, 135, (10), 3768-3771.

### Table of Contents Artwork

